RSC Advances

PAPER

View Article Online
View Journal | View Issue

Cite this: *RSC Adv.*, 2026, **16**, 15076

Recovery of targeted ytterbium ions from chloride mineralization fluids using phosphate polymeric networks

Amal E. Mubark, *[a] Ahmed A. Eliwa,[a] G. A. Dakroury,[b] Ehab A. A. El-Shazly[b] and K. M. El-Azony[c]

Received 6th December 2025
Accepted 10th March 2026

DOI: 10.1039/d5ra09446a

rsc.li/rsc-advances

Numerous specialized scientific initiatives are underway to extract rare earth elements from natural sources using new, easily manufactured, environmentally benign methods that possess favorable economic implications. Monosodium phosphate (MSP) and disodium phosphate (DSP) were produced as effective sorbents for Yb^{3+} ions following gamma irradiation of a mixture containing acrylic acid, dimethyl allyl ammonium chloride, and monobasic and dibasic phosphate salts. The chemical and physical properties of the two phosphate compounds have been thoroughly characterized and validated by several techniques, including EDX, SEM, FT-IR, and TGA–DTA. The investigation of the adsorption coefficients of ytterbium ions indicated that the peak adsorption was 90 mg g^{-1} for mono-phosphate compounds and 95 mg g^{-1} for di-phosphate compounds. Kinetic and thermodynamic analyses validated the chemical characteristics of the adsorption reactions of Yb^{3+} ions on the functional groups present on the adsorbent surfaces, demonstrating the spontaneity and endothermic nature of the adsorption processes.

1 Introduction

Ytterbium (Yb, atomic number 70) is a soft, malleable, and divalent lanthanide metal with a relatively low melting point (824 °C) and density of 6.97 g cm^{-3}.[1] Chemically, Yb readily forms Yb^{2+} and Yb^{3+} ions, with the trivalent state being more stable in aqueous solutions, influencing its coordination behavior. Its chemistry is dominated by the tendency to form complexes with hard donor ligands, and it exhibits moderate reactivity with water and acids. Natural ytterbium is a mixture of seven stable isotopes and is among the least abundant which, together, exist at concentrations of about 0.3 parts per million.[2,3] Ytterbium mining and production is widespread in many countries, most notably China, the United States, Brazil, and India, where mining operations are carried out for many minerals, the most important of which are monazite, euxenite, and xenotime.[4] Ytterbium is mainly used as a source of gamma rays, in highly stable atomic clocks, as a dopant for stainless steel or active laser media, and as a trapped ion suppressor for quantum computing, and is being investigated as a potential replacement for magnesium in high-precision applications.[5–9]

Ytterbium (Yb^{3+}) is a heavy rare earth element of growing technological importance, commonly encountered in complex aqueous matrices during rare earth processing and recycling. Its separation remains challenging due to its similar ionic radius and chemical behavior to neighboring lanthanides, which limits the efficiency of conventional separation techniques. Consequently, selective adsorption using functionalized porous materials has emerged as a promising approach for Yb^{3+} recovery from multi-ion systems. The separation of individual rare earth elements (REEs) presents significant challenges due to their similar chemical and physical properties, particularly their tendency to exist in the +3 oxidation state. This similarity complicates the development of effective separation techniques, which are crucial for various industrial applications. REEs exhibit subtle variations in ionic radii, making their separation difficult as traditional methods often rely on these differences.[10] Also, the complexity of REE sources further complicates large-scale production, necessitating innovative approaches.[11]

The rising demand for rare earth elements (REE) and their compounds in novel materials and technologies has garnered significant interest in recent years regarding their separation and purification from various sources.[12–18] Numerous sample preparation techniques, such as solid phase extraction (SPE), liquid–liquid extraction (LLE), and liquid–liquid–liquid microextraction (LLLME), have been documented. Solvent extraction is unequivocally one of the preferred techniques for the separation of rare earth elements, employing high molecular weight amines, carboxylic acids, tri-*n*-butyl phosphate (TBP), di-(2-

[a]*Semi-Pilot Plant Department, Production Sector, Nuclear Materials Authority, P.O. 11728, El-Maadi, Cairo, Egypt. E-mail: amal_mubark2014@yahoo.com*

[b]*Nuclear Chemistry Department, Hot Laboratories Centre, Egyptian Atomic Energy Authority, P.O. 13759, Cairo, Egypt*

[c]*Radioactive Isotopes and Generators Department, Hot Laboratories Centre, Egyptian Atomic Energy Authority, P.O. 13759, Cairo, Egypt*

ethylhexyl) phosphoric acid (D2EHPA), trialkylphosphine oxides (Cyanex 923), and the extraction behavior of Yb(III) ions utilizing *N*,*N*,*N*′,*N*′-tetrabutylmalonamide (TBMA) and triphenylarsine (TPAs) due to its high selectivity and well-established coordination chemistry involving organophosphorus ligands. Furthermore, synergistic effect is a prominent phenomena in the solvent extraction of REE and was also researched intensively.[19–21] Among these approaches, LLE and SPE are the most extensively utilized for this purpose.[22] Nevertheless, contemporary research initiatives are aimed toward the development of effective, inexpensive, and compact sample preparation technologies named solid phase extraction. The ion exchange separation of individual rare earth elements (REEs) brings both potential and obstacles. Ion exchange procedures can successfully pre-concentrate and fractionate REEs, however difficulties occur due to the complex chemistry of these elements and the existence of contaminants. Ion exchange resins, such as LEWATIT® MDS 200H, demonstrate selectivity for light REEs like La, Ce, Pr, and Nd, obtaining a loading capacity of 0.25 mmol g^{-1} for REEs.[23] Despite the advancements in ion exchange methods, the inherent complexities of REE chemistry and the presence of challenging impurities continue to hinder optimal separation. This underscores the need for continued research into alternate and complementary separation approaches.[24] Extensive research is being conducted on applying adsorption technology on solid surfaces, recognized for its simplicity, cost-effectiveness, and superior performance relative to alternative technologies. Sorbents can be broadly categorized into inorganic, organic, and bio-sorbents.[25,26]

Due to the remarkable consistency of organometallic compounds, many researches have been conducted on the feasibility of extracting metal ions through organometallic compounds.[27] Polyacrylic acid, polyacrylamide, and polymalic acid are examples of organic polymers with good chemical stability and homogeneity that are rarely employed as adsorbents because of their low mechanical strength. As a result, numerous investigations into increasing their mechanical strength through compound combinations have been conducted.[28] It was also necessary to preserve these produced compounds' high stability and resistance to chemicals and physical changes when combined with different acidic media. The primary prerequisites for such advancements in the production of adsorbents were cheap cost and ease of synthesis.

Different authors studied the separation process of rare earths from the chloride solution using different organic extractants such as anionic, cationic, or solvating types depending on the ions present in the solution. Cationic extractants are superior in the extraction and separation of lanthanides as they form cationic species in an aqueous chloride solution. Organophosphorous acids, such as di(2-ethylhexyl)phosphoric acid (D2EHPA) and 2-ethylhexyl 2-ethylhexylphosphonic acid (HEHEHP/PC 88A), are suitable extractants for the separation of rare earth metals from chloride solutions.[29] Organophosphoric acids are characterized by the presence of phosphate groups, which are the functional groups responsible for interactions with rare earth metal ions during adsorption processes. Therefore, it was considered to invent and synthesize compounds containing phosphate groups as adsorbents for ytterbium as a lanthanide element, with the possibility of benefiting from synthesizing these materials in a solid, polymerized form. Although multidentate ligands have demonstrated excellent selectivity in liquid–liquid extraction systems, their application is often limited by solvent consumption, phase disengagement issues, and operational complexity. In contrast, porous networks enable solid–liquid extraction with high surface accessibility, tunable pore architecture, and enhanced stability, providing a more sustainable and reusable platform for metal ion separation.

In this work, a mixture of acrylic acid and allyl alcohol in the presence of mono- or di-sodium phosphate was gamma-irradiated to produce two compounds, MSP and DSP. They were investigated for possible applications as Yb^{3+} adsorbents from chloride media. The kinetics and thermodynamic results of the coefficients affecting Yb ion adsorption on MSP and DSP composites were examined and calculated. Studies on stability, recycling, and desorption were also carried out for both sorbents. Additionally, the efficacy of the MSP and DSP composites was assessed by recovering the ytterbium content from real sample chloride fluids, analyzing the influence of competing elements on the adsorption efficiencies of Yb^{3+} ions on both phosphate composites, and testing their selectivity.

2 Materials and methods

2.1. Reagents and materials

Ytterbium oxide (Yb_2O_3, 99.9%) was used as and Yb^{3+} ion source and obtained from MERCK, Germany. Acrylic acid a monomer ($C_3H_4O_2$, 99%) and dimethyl allyl ammonium chloride were purchased from MERCK, Germany. The cross-linker *N*,*N*′-methylene bisacrylamide MBA ($C_7H_{10}N_2O_2$, 99%) was produced by Merck, Germany. Double distilled water (DDW) was utilized in this investigation. Merck provided the hydrochloric acid (HCl), sulfuric acid (H_2SO_4), and sodium hydroxide (NaOH) used in this investigation's pH changes and regeneration. To prepare 1000 mg L^{-1} of ytterbium for batch adsorption investigations, 0.114 g of ytterbium oxide was fully dissolved in 2 mL of concentrated hydrochloric acid with three drops of concentrated nitric acid and diluted to 100 mL. The prior solution was diluted with DDW to create the appropriate concentrations. In order to prevent sedimentation brought on by raising the pH level, the precipitation limits of Yb^{3+} ions were taken into account. This could prevent the confusion between the deposition of metal ions at high pH values and their adsorption on the phosphate composites.

Two mineralization samples were collected and subjected to several physical and hydrometallurgical treatments from NMA.[30,31] The non-magnetic portions of the two regions were digested with sodium hydroxide at 623 K in a furnace. The digested fractions were subjected to two stages of leaching, first leaching with hot DDW and then leaching with dilute hydrochloric acid (30%) at 363 K for 2 hours. Two chloride solutions containing a specified concentration of Yb^{3+} ions were obtained. The recovery of Yb^{3+} contents of the two feed solutions

was studied using phosphate composites prepared under the optimum conditions obtained through the study.

2.2. Preparation of the phosphate composites

Two composite materials were synthesized *via* free radical polymerization, one using monosodium phosphate and the other using disodium phosphate. In both cases, 5 g of acrylic acid (AA), 20 g of dimethyl allyl ammonium chloride, and 0.1 g of *N*,*N*′-methylene bisacrylamide as a cross-linking agent were employed.

2.2.1. Monosodium phosphate composite (MSP). In the first preparation, 7.4211 g of monosodium phosphate was used. The monomers were dissolved in 50 mL of deoxygenated water to ensure a uniform mixture. The solution was then irradiated with 25 kGy of gamma radiation using a ^{60}Co source at the Cyclotron Project, Inshas site, Egypt.[32] Gamma irradiation initiated the polymerization process, promoting cross-linking between acrylic acid, dimethyl allyl ammonium chloride, and DAM and forming long polymer chains. To remove impurities and unreacted components, the final product was chopped into tiny pieces and immersed in acetone for two hours after polymerization. Following a 24-hour drying process at 333 K in a vacuum oven, the composite was ground using an electric grinder and sieved to a particle size of 300 μm. The particle size of 300 μm was selected to provide an optimal compromise between enhanced surface area and minimized intraparticle diffusion limitations, while maintaining sufficient mechanical stability and ease of solid–liquid separation during adsorption experiments. Finer particles may increase surface area but can lead to aggregation and handling difficulties, whereas larger particles may reduce adsorption kinetics due to increased diffusion resistance.

2.2.2. Disodium phosphate composite (DSP). In the second preparation, 4.3904 g of disodium phosphate was used instead of monosodium phosphate. The preparation method remained identical: the monomers were dissolved in 50 mL of deoxygenated water, irradiated with 25 kGy of gamma radiation, and allowed to polymerize. The polymerized material was cut into small pieces, soaked in acetone for 2 hours, dried in a vacuum oven at 333 K for 24 hours, and milled to a particle size of 300 μm.

After drying, the polymer composites were ground and sieved to obtain a uniform particle size of 300 μm, which was used in all adsorption and kinetic experiments to minimize particle-size-dependent mass transfer effects. Both composites feature functional groups, including carboxyl (–COOH), hydroxyl (–OH), and phosphate groups, providing active sites for the adsorption of metal ions.

2.3. Instrumentation and characterization

The functional groups present in the mono- and di-phosphate compounds were identified using Fourier transform infrared (FTIR) spectroscopy (Bomen Mickelson, model MB157, Canada). The crystal structure of the prepared composites was evaluated using X-ray diffraction (XRD), Shimadzu, Model XD-Dl, Kyoto, Japan. The phase and mass variations from 20 to 600 °C were examined using a DTA-TGA system of type DTA-TGA-50, Japan. The components and morphology of phosphate composites were examined using a scanning electron microscope model JEOL-JSM-5600LV (FEI Quanta FEG-250, EDX), JEOL Ltd from Japan. The BET surface area, the pore size distribution, and N_2 adsorption–desorption isotherms of the MSP and DSP composites were determined using a surface area analyzer (Nova 3200 series, Micrometric) (USA). During this study, the concentrations of Yb^{3+}, Ca^{2+}, Fe^{3+}, V^{4+}, and Nb^{5+} ions were measured using appropriate spectroscopic methods using a UV-vis spectrophotometer model SP-8001, Metretech Inc., China.[33] The concentration of Na^{+} ions was determined using a Sherwood Scientific Flame Photometer Model 410, UK.

2.4. Batch adsorption tests

As indicated in Table 1, a number of factors were examined in order to examine the potentiality and recovery behavior of Yb^{3+} ions on the mono- and di-phosphate composites. Each experiment involved mixing 0.01 g of produced composite with 10 mL of a chloride solution with a certain concentration of Yb^{3+} ions in 50 mL glass flask bottles. The mixture was then agitated at 300 rpm for a predetermined number of minutes. To enhance the ytterbium ion recovery procedures, a number of variables in variable ranges, including aqueous phase pH, adsorption period, metal ion concentration, and composite dose, were investigated. Wattman filter paper was used for the solid/liquid separation (filtration) procedures once the stirring period had passed. It was determined how much ytterbium was present in the remaining effluent solutions. Eqn (1)–(3) were used to calculate the recovery efficiencies based on the concentrations.

$$\text{Recovery efficiency}(\%) = \left(\frac{C_o - C_e}{C_o}\right) \times 100 \quad (1)$$

$$q_t = (C_o - C_t) \times \frac{V}{m} \quad (2)$$

$$q_e = (C_o - C_e) \times \frac{V}{m} \quad (3)$$

where the amounts of Yb^{3+} ions on the composite at equilibrium time and time t (min) were denoted by q_e and q_t (mmol g^{-1}), respectively. The initial and equilibrium concentrations of Yb^{3+} ions were C_o and C_e (mmol L^{-1}), respectively. Additionally, C_t showed the concentration of Yb^{3+} ions in the aqueous phase at time t. V and m denoted the feed solution's volume (L) and the solid composite's mass (g), respectively. To get the average results using the standard deviation, each experiment was conducted three times. Using a specific concentration of one of the coexisting elements Na^{+}, Ca^{2+}, Fe^{3+}, V^{4+}, and Nb^{5+} ions, the competing ions effect was thoroughly investigated. Using the best other conditions previously attained during the study, equal concentrations of competing metal ions and ytterbium were combined to assess the impact of their presence on the recovery efficiencies of ytterbium. Table 1 lists the parameters that were examined, the degree to which these elements changed, and the additional fixed circumstances that were present during the investigation of each influencing factor.

Table 1 Adsorption parameters of Yb^{3+} ions on the MSP and DSP composites

Adsorption parameters	Average of change	Conditions
pH	1–5	0.01 g Sorbent, 10 mL liquid, 100 mg per L Yb^{3+}, 298 K, and 60 min
Time, min	5–120	0.01 g Sorbent, 10 mL liquid, 100 mg per L Yb^{3+}, 298 K, and pH = 4
Sorbent dose, g	0.01–0.05	10 mL Liquid, 100 mg per L Yb^{3+}, 298 K, pH = 4, and 45 min
Metal ion conc., mg L^{-1}	25–200	10 mL Liquid, 298 K, pH = 4, 45 min, and 0.01 g sorbent
Stirring temp., K	298–328	10 mL Liquid, pH = 4, 45 min, 0.01 g sorbent, 100 mg L^{-1} and Yb^{3+}
Competing ions	Na^{+}, Ca^{2+}, Fe^{3+}, V^{4+}, and Nb^{5+}	10 mL Liquid, pH = 4, 45 min, 0.01 g sorbent, 100 mg per L Yb^{3+}, and 298 K

2.5. Adsorption kinetics and thermodynamics

2.5.1. Kinetic modeling of Yb^{3+} adsorption. Pseudo-1st-order, pseudo-2nd-order, Elvoich, and intraparticle diffusion models could be used to represent the sorption rate determination step for Yb^{3+} onto MSP and DSP composites and the order of their interactions.

2.5.2. Pseudo-1st and 2nd order models. Pseudo-1st-order kinetics applied in the non-linear form is shown in eqn (4).

$$q_t = q_{e(cal.)}(1 - e^{-k_1 t}) \quad (4)$$

The pseudo-2nd-order model (in the non-linear form) is shown in eqn (5).

$$q_t = ((k_2 {q_{e(cal.)}}^2 t)/(1 + k_2 q_e t)) \quad (5)$$

The pseudo-1st-order rate constant was denoted by k_1. The adsorbed amounts at time t and equilibrium were, respectively, q_t and $q_{e(cal.)}$. The pseudo-2nd-order kinetic constant was represented by k_2.[34]

2.5.3. Elvoich model. The chemisorption reaction's compatibility with second-order kinetics was demonstrated by the Elvoich model. Eqn (6) could be used to depict the Elvoich model's non-linear form.

$$q_t = 1/\beta \ln(1 + \alpha\beta t) \quad (6)$$

where the Elovich constants were represented by α and β. β was the desorption constant (g mg^{-1}), and α was the Elovich initial adsorption rate (mg g^{-1} min^{-1}).[35]

2.5.4. Intraparticle diffusion model. The intraparticle diffusion model is often used to explain how adsorption works, especially in porous materials. It describes how adsorbate molecules travel into the inner pores of a sorbent. Adsorption typically happens in three steps: first, the adsorbate molecules move from the bulk solution to the outer surface of the sorbent (film diffusion); next, they travel into the pores of the sorbent (intraparticle diffusion); and finally, they attach to active sites on the sorbent. The slowest step controls the overall rate of the process. The intraparticle diffusion is represented by eqn (7).

$$q_t = k_i t^{0.5} + C \quad (7)$$

where k_i is the intraparticle diffusion rate constant (kg^{n-1} g^{1-n} min^{-1}), C indicates the thickness of the boundary layer (mg g^{-1}). A larger C suggests a greater influence of the surface process.

2.5.5. Thermodynamics studies. The temperature factor results were used to explore thermodynamic investigations of the Yb^{3+} ion adsorption processes on the MSP and DSP composites. The Van't Hoff equation (eqn (8)) was used to compute the enthalpy and entropy changes for the sorption processes.[36] Eqn (9) was used to determine the Gibbs free energy changes of the adsorption processes.

$$\ln K_d = \frac{\Delta S}{R} - \frac{\Delta H}{RT} \quad (8)$$

$$\Delta G = \Delta H - T\Delta S \quad (9)$$

In this case, $\Delta H°$ (kJ mol^{-1}), $\Delta S°$ (kJ mol K^{-1}), and $\Delta G°$ (kJ mol^{-1}) represented enthalpies, entropy changes, and Gibbs free energy changes, respectively. The temperature and the gas constant were T (K) and R (J K^{-1} mol^{-1}).

To find the best-fit model for the sorption process, quantitative error functions such as chi-square (χ^2) and coefficient of determination R^2 were calculated for the modeling data. The best-fit model has a minimum value of χ^2 and a maximum value of R^2, which is close to unity. The two equations used to calculate the R^2 and χ^2, respectively, were represented by eqn (10) and (11).[37]

$$R^2 = 1 - \frac{\sum_{i=1}^{n} (q_{calc.} - q_{exp.})^2}{\sum_{i=1}^{n} (q_{calc.} - q_{mean})^2} \quad (10)$$

$$\chi^2 = \sum \frac{(q_{calc.} - q_{exp.})^2}{q_{calc.}} \quad (11)$$

where $q_{exp.}$, $q_{calc.}$, and q_{mean} (mg g^{-1}) represented the amount of ions adsorbed, the anticipated amount of adsorbed ions, and the average of the ions' q_{exp} values, respectively.

2.6. Desorption tests and application on actual chloride fluids

To determine the best elution conditions, the desorption processes of Yb^{3+} ions from the loaded MSP and DSP composites were examined. Two strengths of sulfuric and hydrochloric acids (0.5 and 1.0 mol L^{-1}) were used for the elution investigations on the loaded phosphate composites. Several stationary conditions, including 0.05 g loaded sorbent, 10 mL acid solution, and 30 minutes of stirring at 300 rpm at room temperature, were used for the elution tests. Following each experiment,

the spent MSP and DSP compounds were filtered, and their elution efficiencies were calculated using eqn (12) by measuring the concentration of Yb^{3+} ions in the filtrate solution.

$$\text{Desorption efficiency} = \left(\frac{C_e}{C_L}\right) \times 100 \quad (12)$$

where C_e and C_L represented the Yb^{3+} metal ion concentrations on the adsorbent prior to elution and in the aqueous phase following elution, respectively.

Two mineralization samples were gathered and put through a number of physical and hydrometallurgical processes at the Nuclear Materials Authority's research facilities at the Inshas location in Egypt. The two areas' non-magnetic parts were broken down in a furnace at 623 K using sodium hydroxide. The digested fractions were leached twice: once using hot DDW and again for two hours at 363 K using diluted hydrochloric acid (30%). Two chloride solutions with a given Yb^{3+} ion concentration were produced. Along with other metal ions, the feed solutions had reasonable amounts of Yb^{3+} ions. Phosphate composites made under the ideal circumstances discovered during the investigation were used to examine the recovery of Yb^{3+} contents of the two feed solutions. The efficiency of the MSP and DSP composites as Yb^{3+} ion sorbents and the impact of competing elements on their selectivity and adsorption efficiencies were assessed.

3 Results and discussion

3.1. Characteristics of the MSP and DSP composites

3.1.1. XRD results. The X-ray diffraction (XRD) patterns of the MSP and DSP adsorbents reveal their predominantly amorphous structural nature (Fig. 1). The MSP diffractogram exhibits a broad and low-intensity hump centered between $2\theta \approx$ 15–30°, without any sharp crystalline peaks, indicating a largely disordered structure with minimal long-range atomic ordering. This amorphous character is typical of materials derived from biological or polymeric origins, which often contain irregular networks of organic and inorganic constituents. Similarly, the DSP pattern shows a slightly more pronounced broad hump between $2\theta \approx$ 15–35°, suggesting a partially amorphous matrix with slightly higher structural ordering compared to MSP, possibly due to thermal or chemical modifications during preparation. The absence of well-defined crystalline peaks in both materials confirms that they lack significant crystalline domains, which may enhance their surface heterogeneity and availability of active sites for adsorption processes. Such amorphous morphology is advantageous for adsorbent materials because it increases the number of functional groups and pores accessible for contaminant binding.[38]

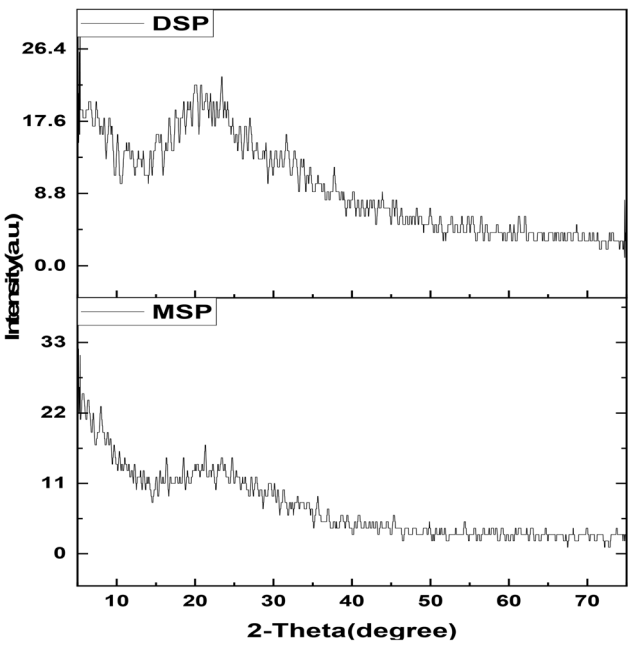

Fig. 1 XRD pattern of the MSP and DSP composites.

3.1.2. EDX results. As predicted, carbon and oxygen were the main constituents of the synthesized mono- and di-phosphate sorbents as shown in Fig. 2. In addition, remarkable peaks have appeared for phosphorous in the EDX-charts of the loaded and unloaded sorbents which proved the interaction between sodium phosphates and the other added monomers especially acrylic acid as discussed in the synthesis and adsorption mechanism section. As shown in Fig. 2b and d, obvious decreases in the percentages of C, O, and P were observed due to the pronounced presence of Yb^{3+} ions, proving their recovery on the surfaces of phosphate composites. However, the appearance of many elements in the EDX-plots such as Na and Cl can be attributed to the use of sodium hydroxide and hydrochloric acid throughout the experiments, which requires more washing steps. The higher appearance of Yb on the EDX plot of DSP-Yb compared to MSP-Yb as shown in Fig. 2b and d was attributed to the higher presence of chloride in the EDX plot of MSP-Yb which reduced the percentages of Yb and also affected the percentages of C and O.

3.1.3. Morphology results. Fig. 3 illustrates the morphology of the synthesized phosphate composites before and after adsorption. Randomly assembled particles of mono- and di-phosphate sorbents appeared forming large agglomerations of heterogeneous shapes and a non-uniform size range in diameters. However, the spherical appearance of the di-phosphate was more than that of the monophosphate and its homogeneity was relatively remarkable. This could be attributed to the higher interaction between the carboxylic groups present in the polymer structure and sodium di-phosphate compared to sodium mono-phosphate. Many random corrugated cavities and cracks were observed in the composites. White scattered particles appeared on the surface of the loaded MSP and DSP composites as shown in Fig. 3b and d. These spots demonstrated the adsorption of ytterbium ions on the surfaces of the composite materials and the entrapping of the recovered ions across the active sites of the MSP and DSP sorbents. Fig. 3b–d shows a hypothetical wave-like layer composed of surfaces with a marked lack of interstitial voids, which are reduced on the outer surface due to the adsorption of Yb^{3+} ions. On the other hand, as shown in Fig. 3a and c, the unloaded

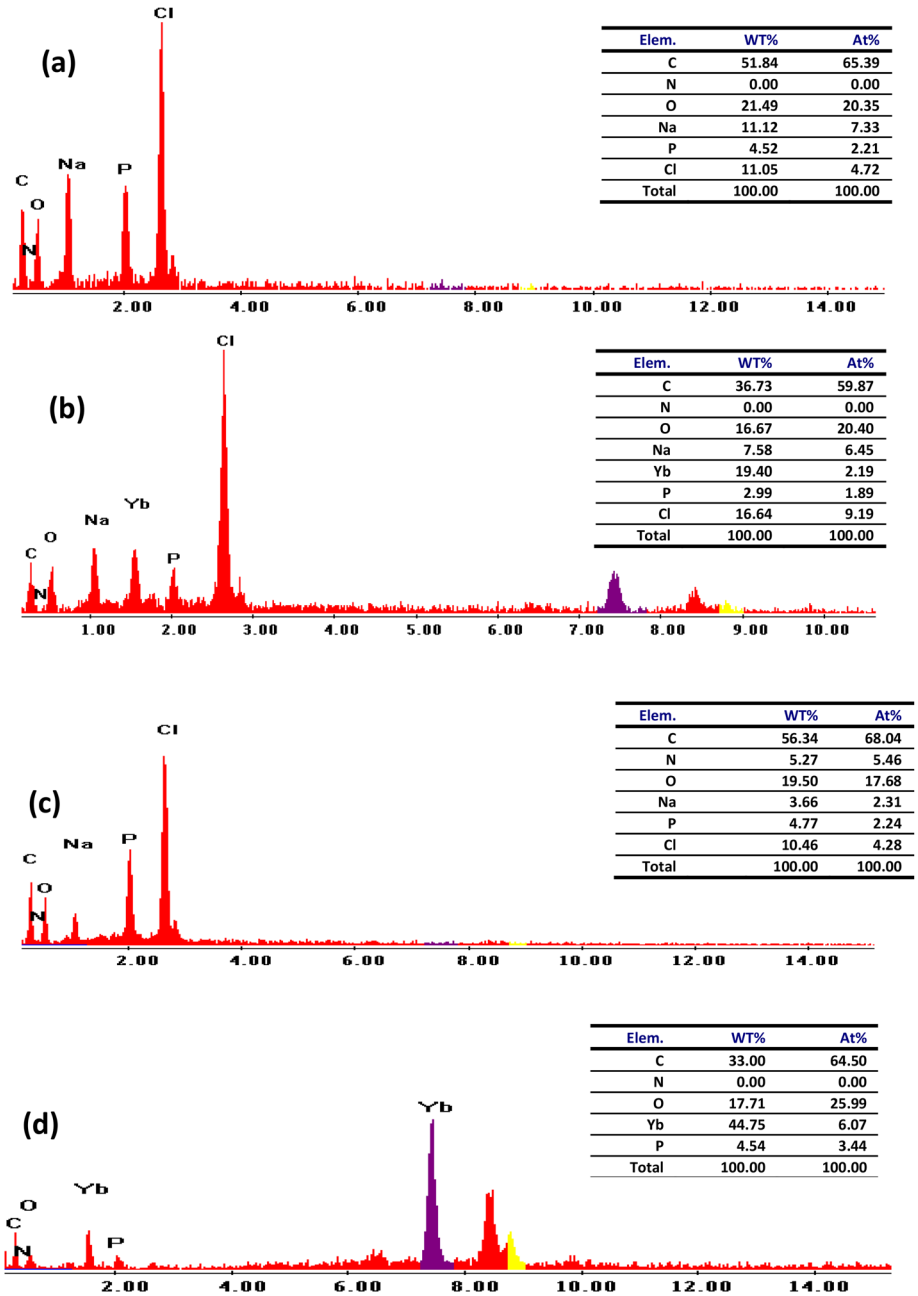

Elem.	WT%	At%
C	51.84	65.39
N	0.00	0.00
O	21.49	20.35
Na	11.12	7.33
P	4.52	2.21
Cl	11.05	4.72
Total	100.00	100.00

Elem.	WT%	At%
C	36.73	59.87
N	0.00	0.00
O	16.67	20.40
Na	7.58	6.45
Yb	19.40	2.19
P	2.99	1.89
Cl	16.64	9.19
Total	100.00	100.00

Elem.	WT%	At%
C	56.34	68.04
N	5.27	5.46
O	19.50	17.68
Na	3.66	2.31
P	4.77	2.24
Cl	10.46	4.28
Total	100.00	100.00

Elem.	WT%	At%
C	33.00	64.50
N	0.00	0.00
O	17.71	25.99
Yb	44.75	6.07
P	4.54	3.44
Total	100.00	100.00

Fig. 2 EDX charts of the (a) MSP, (b) MSP-Yb, (c) DSP, and (d) DSP-Yb sorbents.

manufactured composites appeared as semi-spherical shapes with variation in size.

3.1.4. FTIR results. One of the most important techniques for chemical analysis was FT-IR spectroscopy, which monitored the functional groups and different bonds of the compound under study and subsequently demonstrated the anticipated composition of the manufactured product. Fig. 4 displayed the FT-IR curve of the MSP and DSP composites both before and after the Yb^{3+} ions were absorbed. While exhibiting unique banding with some variations, the composites' spectra were quite comparable. First, the adsorption of Yb^{3+} on the composite adsorbent was indicated by the decrease in the intensity of the bands of the representative functional groups and the increase in the intensity of the metal ions-active sites interaction bands (M–O). Three separate zones were identified in the phosphate composites' resultant spectra. The O–H of hydroxyl groups and the phosphinic acid and C–H stretching vibrations, respectively, are represented by the high-energy bands in the first area, which spanned from 3420 to 2927 cm^{-1}.[39–41] The carbon dioxide from the air may be responsible for the bands that formed at 2360 cm^{-1}.[42] The C=O and COO-bands of acrylic acid or ketones showed a slight fluctuation in intensity at 1736 cm^{-1} on the middle energy range, whereas the intense band of the OH and C=O groups

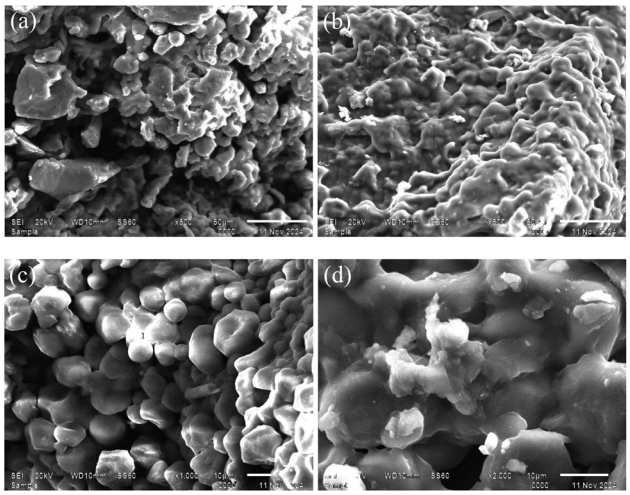

Fig. 3 SEM images of the (a) MSP, (b) MSP-Yb, (c) DSP, and (d) DSP-Yb sorbents.

showed a strong, sharp variation at 1636 cm^{-1}.[43] The interaction between Yb^{3+} ions and the high density hydroxyl or carboxyl groups found in the composite skeletons may be seen by these variations in peak intensity. The P═O and P–OH bands of the phosphate group in the complex were identified as the bands with wavenumbers 1159 and 1015 cm^{-1}. These bands significantly changed following loading with Yb ions, demonstrating the interaction between the polyvalent cations and the phosphate groups.[44,45] The M–O combination is responsible for the band's disappearance or decrease in the low energy region at 1159, 1079, and 1015 cm^{-1} following ytterbium ion loading.[46] Lastly, interactions between metal ions and the composite's carboxylic groups can be responsible for the distortion or drop in strength of the COO groups bands seen at 620 cm^{-1}. The most pronounced spectral changes occurred in the phosphate region. The P═O and P–OH stretching bands at 1159 and 1015 cm^{-1} underwent significant intensity decrease and partial shifting after Yb^{3+} adsorption, accompanied by changes in the M–O region at 1079 cm^{-1}. These observations indicate that the Yb^{3+} ions coordinate primarily with the phosphate groups, forming strong metal–phosphate interactions. Minor shifts in the COO^{-} bands at 620 cm^{-1} suggest that carboxylate groups may play a secondary or stabilizing role, but phosphate groups are the dominant binding sites. Overall, FT-IR confirms that ytterbium adsorption is mainly governed by coordination to the phosphate groups of the polymer network, with additional weaker interactions with carboxylate groups contributing to overall metal ion stabilization.

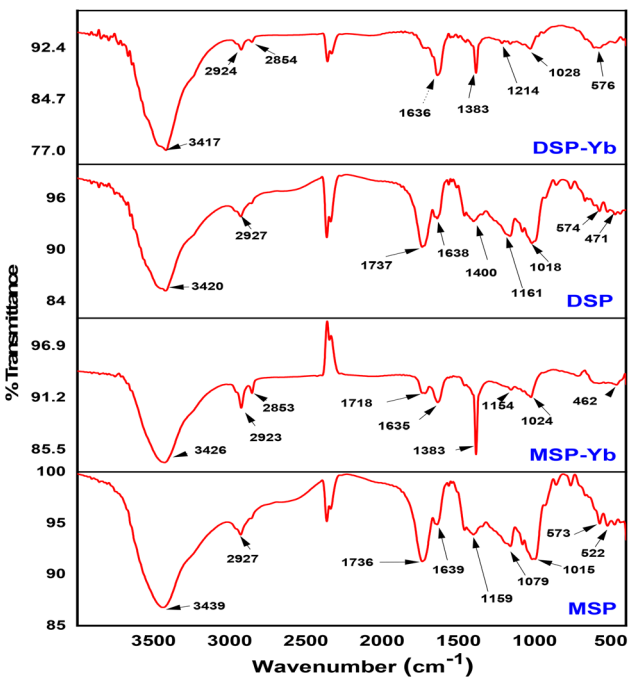

Fig. 4 FTIR spectra of the loaded and unloaded MSP and DSP.

While solid-state ^{31}P NMR was not performed in this study, the synthesis approach *via* gamma-irradiation-induced free-radical polymerization is known to promote covalent integration of functional monomers into acrylic polymer backbones. The monomers and phosphate additives are expected to react through radical-mediated grafting and cross-linking rather than being physically entrapped. Additionally, the composites underwent thorough washing with acetone to remove unreacted monomers and physically adsorbed phosphate salts. Together with the observed phosphate-related functional groups in FT-IR, these factors strongly suggest covalent incorporation of phosphate into the polymer network. Future work will include solid-state ^{31}P NMR measurements to definitively confirm covalent bonding and distinguish it from any residual physically trapped phosphate species.

3.1.5. Thermal analysis findings. Thermogravimetric analyses (TGA) were used to quantify the endothermic and exothermic phase transitions of the synthesized polymers and to forecast their performance and chemical degradation characteristics. Fig. 5 showed the phosphate composites' phase transitions and heat stability. The MSP composite's TGA curve revealed four mass loss stages and an overall mass drop of 99.14%, whereas the DSP composite's TGA curve revealed three mass loss stages and an overall mass decrease of 99.53%. These significant mass losses demonstrated their poor thermal stability, which was explained by the sorbent structure's high organic composition. For MSP and DSP composites, the first stage, which lasted from 30 to 200 degrees Celsius, produced a comparatively little loss of resin mass of roughly 4.58 and 6.02%, respectively. For MSP and DSP composites, this stage was accompanied by an endothermic peak at 144 and 160 °C, respectively, which was ascribed to the elimination of chemically bounded water (water of hydration).[47] The temperature rise from 200 to 340 °C caused a second large drop in the mass of MSP and DSP composite materials, which was 84.69 and 85.92%, respectively. This is explained by the removal of carboxyl groups that produce carbon dioxide gas during combustion and the water of crystallization.[48,49] This combustion caused a discernible shift in the DTA curve, which produced an endothermic peak as seen in Fig. 5. This was assumed to be the result of the burning of distinct organic

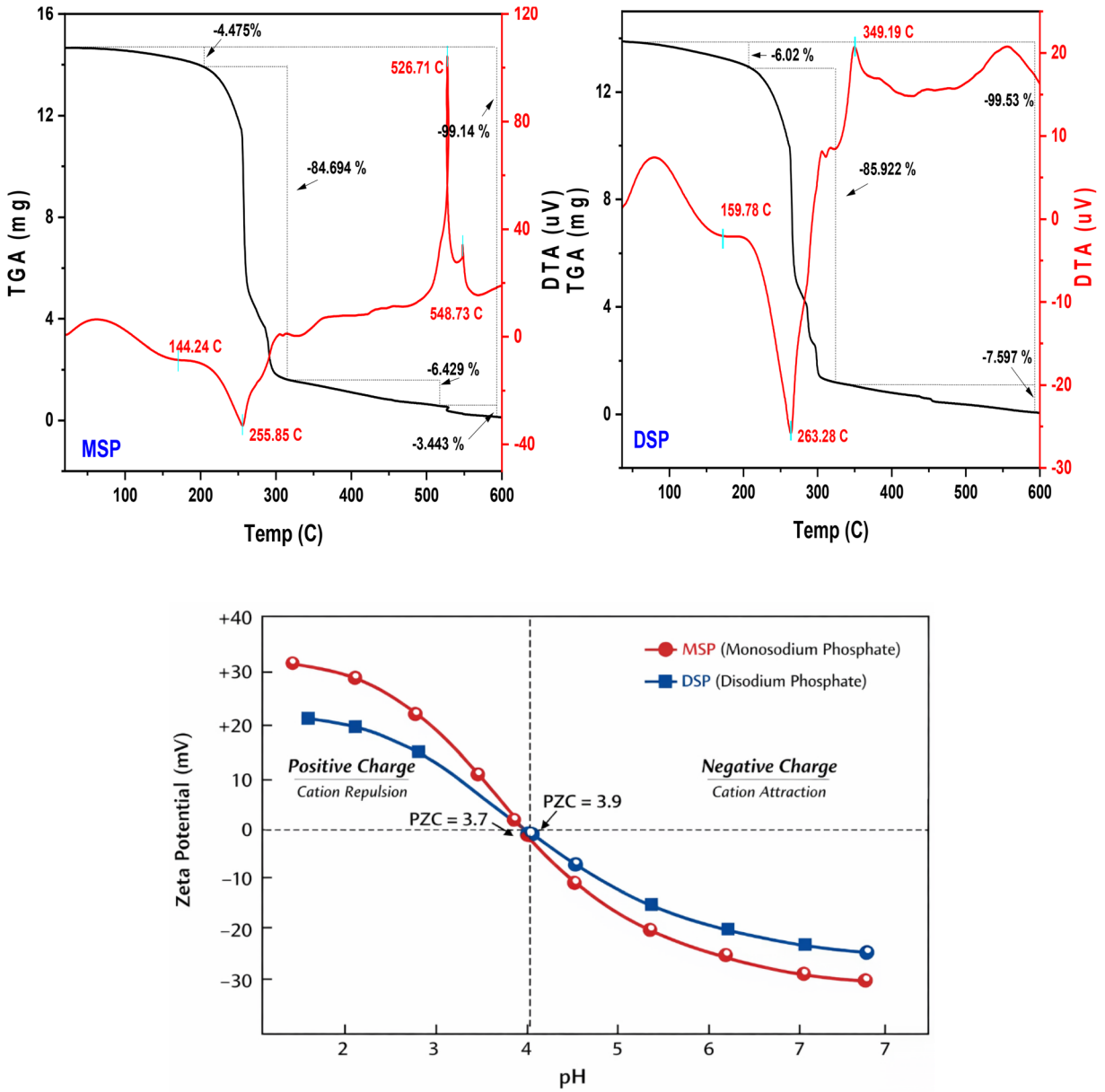

Fig. 5 DTA–TGA chart of the MSP and DSP composites; zeta potential *vs.* pH for MSP and DSP composites.

substances leading the creation of different. In the third stage, the TGA curves showed a mass loss of roughly 6.23 and 7.59% for MSP and DSP composites, respectively, when the temperature was raised from 340 to 507 or 600 °C. This could be explained by the combustion of the composite's residual hydrocarbon content, which resulted in the total removal of the organic content and the production of phosphate ashes.[50] Because the phosphate content was incombustible, the resins' low thermal durability up to 600 °C led to solid residues of less than 1% of the initial resin weight.[51]

3.1.6. Zero point charge (PZC). Zeta potential measurements of MSP and DSP composites were performed over a pH range of 2–7 to determine the point of zero charge (PZC) as shown in Fig. 5. The PZC values were found to be 3.7 for MSP and 3.9 for DSP, confirming that at pH 4.0, the composite surfaces are slightly negatively charged, validating that electrostatic attraction is the primary mechanism for cation adsorption.

3.2. Optimization of adsorption experiments

3.2.1. Effect of pH. The impact of pH on adsorption processes has been extensively researched because it directly affects the metal ion speciation and the protonation of active sites on the adsorbent surface.[48] Chloride solutions with pH values ranging from 1.0 to 5.0 were used to examine these effects. We chose pH 5 as the pH ceiling for the tests because of the deposition threshold at which ytterbium precipitates as $Yb(OH)_3$ begins to occur, which influences the adsorption efficiency calculation, as shown in Fig. 6. This led us to investigate

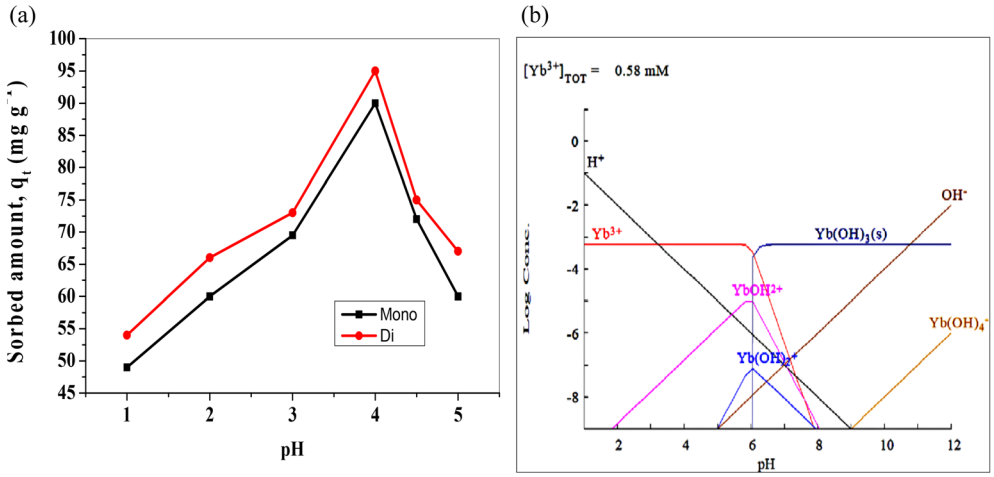

Fig. 6 (a) Effect of pH on the adsorption of Yb^{3+} on the MSP and DSP composites, (b) speciation of ytterbium at different pH.

its effect over this range. MEDUSA software was used to run simulations in order to confirm the chemical formulae of ytterbium species ions in the feed solutions (Fig. 6c). As seen in Fig. 6b, Yb^{3+} ions predominated, with $YbOH^{2+}$ ions and positive hydrogen ions appearing comparatively weakly in the examined range. By varying the pH of feed solutions from 1.0 to 4.0, which is thought to be the ideal pH value for both composites and would be applied in the following parameters, Fig. 6a showed significant increases in the adsorption of Yb^{3+} on both phosphate composites, ranging from 49 to 90 mg g^{-1} and from 54 to 95 mg g^{-1}. The observed decrease in competing hydrogen ions with rising pH, which offers more opportunities for the adsorption of ytterbium ions to the active sites on the composite surfaces, was the reason for the rise in the adsorption efficiency of Yb^{3+} ions utilizing the MSP and DSP.

3.2.2. Influence of time and kinetic modelling. Since all adsorption experiments were conducted using composites with identical particle size (300 μm), variations in adsorption kinetics are attributed to differences in chemical functionality and phosphate incorporation rather than particle size or diffusion limitations. Studying the adsorption of Yb^{3+} ions on the phosphate sorbents as a function of time could help us understand the adsorption processes' kinetics. In addition, as shown in Fig. 7, the equilibrium time of the adsorbent–adsorbate interaction and maximum uptake of Yb^{3+} ions on the MSP and DSP composites were studied and determined using other constant conditions as illustrated in Table 1. These studies were performed using different contact times ranging from 5 to 120 min using 10 mL of chloride solutions with pH 4.0, 100 mg per L Yb^{3+} concentration, 0.01 g per L solid fractions of MSP and DSP separately, and at ambient temperature. Fig. 7 demonstrated that the maximum adsorption (q_e) of MSP and DSP phosphate adsorbents for Yb^{3+} ions was 90 and 95 mg g^{-1} after 45 minutes, respectively. As shown in Fig. 7a, adsorption proceeds in two stages. The initial rapid uptake corresponds to surface binding and film transport of Yb^{3+} ions to readily accessible phosphate sites. This stage is driven by the high concentration gradient and the abundance of unoccupied active

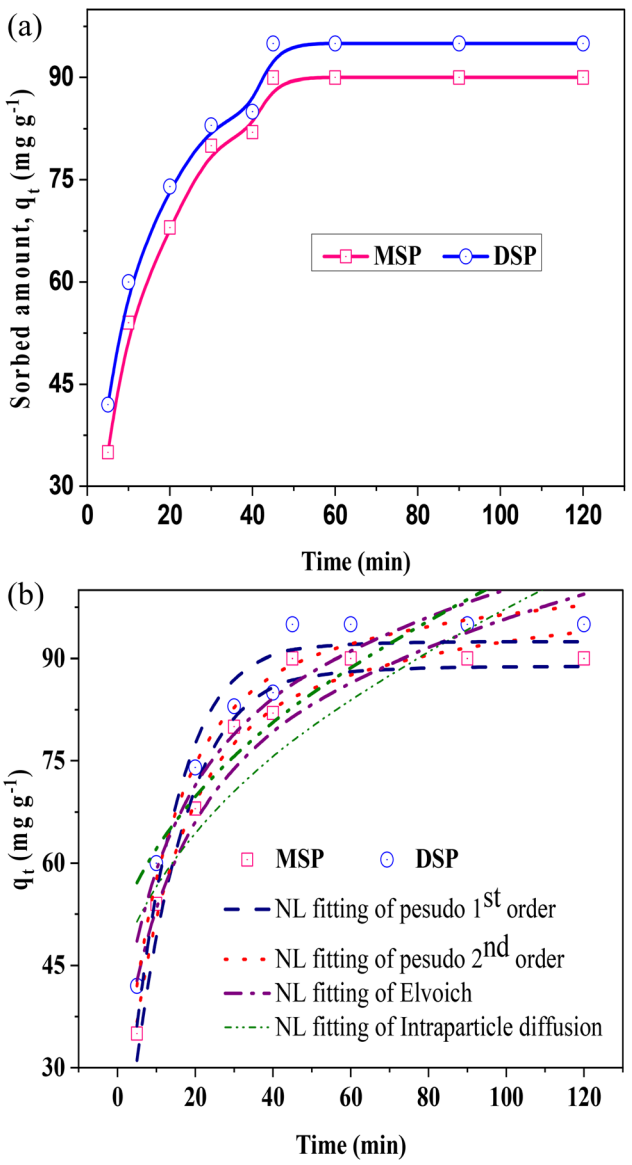

Fig. 7 (a) Effect of time on the adsorption of Yb^{3+} on the MSP and DSP composites and (b) the plotting of non-linear kinetics models.

Table 2 Calculated kinetic parameters for Yb^{3+} sorption onto MSP and DSP composites[a]

	Kinetic model	
	Sorbate	
Parameters	Mono	Di
Quasi-1st-order		
q_t (mg g^{-1}) (calculated)	88.833 ± 1.648	92.445 ± 2.1649
k_1 (min^{-1})	0.08613 ± 0.00697	0.09909 ± 0.01077
R^2	0.9692	0.9353
χ^2	11.792	22.76072
Quasi-2nd-order		
q_t (mg g^{-1}) (calculated)	100.724 ± 2.36898	103.755 ± 2.08999
k_2 (g mg^{-1} min^{-1})	0.00114 ± 1.466 × 10^{-4}	0.00131 ± 1.53844 × 10^{-4}
R^2	*0.9753*	*0.9758*
χ^2	*9.47043*	*8.5083*
q_t (mg g^{-1}) (experiment)	**90**	**95**
Elvoich		
A	33.82856 ± 16.0049	51.55064 ± 24.4009
B	0.05431 ± 0.0077	0.05657 ± 0.00715
R^2	0.891	0.90445
χ^2	41.639	33.58783
Intraparticle diffusion		
k_{iD}	32.847 ± 5.657	37.66803 ± 5.3434
C	0.2336 ± 0.0437	0.21354 ± 0.3624
R^2	0.81612	0.83998
χ^2	70.384	56.253

[a] The highest R^2 and the lowest χ^2 are in bold and italicized.

sites. The subsequent slower stage reflects diffusion of Yb^{3+} ions within the hydrated cross-linked polymer network toward less accessible internal phosphate groups, rather than classical pore diffusion in a rigid porous solid. As adsorption progresses, the decreasing availability of active sites and increased diffusion path length within the polymer matrix lead to a gradual approach to equilibrium.

On the other hand, Fig. 7b showed the plot of nonlinear kinetic models for the adsorption processes of Yb^{3+} ions on MSP and DSP compounds. In addition, Table 2 detailed the kinetic parameters of the applied models, namely Pseudo-1st-order, Pseudo-2nd-order, Elvoich, and Intraparticle diffusion models. Regarding the calculated pseudo-first-order and pseudo-second-order q_t, their values were closer to the experimental q_t for Yb^{3+} adsorption for the two phosphate sorbents. Additionally, when applying the error functions R^2 and χ^2 to choose the best fitting mode, the second pseudo-order was the more fitted model with lower values of the error function χ^2 for both sorbents. This implied that the adsorption of Yb^{3+} ions on MSP and DSP was chemically mediated. Therefore, the low performance of R^2 and its inadequacy for the nonlinear regression model were revealed.[52]

3.2.3. Influence of sorbent dose. A study was carried out utilizing various amounts of manufactured sorbents ranging from 0.01 to 0.05 g to find the optimal quantity of phosphate compounds capable of absorbing the maximum Yb^{3+} ions under otherwise constant conditions. The sorbent dosage impact investigation also included 10 mL of an aqueous solution with a concentration of 100 mg per L Yb^{3+}, a pH of 4.0, and stirring for 45 minutes at room temperature. It has been established that the adsorption effectiveness increases with the weight of the adsorbent material for fixed metal ion concentrations. On the other hand, sorbent uptakes decrease with increasing adsorbent material weight. In other words, large uptakes (q_e) are associated with small sorbent dosages that have poorer absorption efficiency. According to the results shown in Fig. 8a, increasing the solid mass from 0.01 to 0.05 g resulted in significant reductions in the uptakes of Yb^{3+} ions on MSP and DSP phosphate composites. The decrease in adsorption capacity with increasing sorbent dose is attributed to depletion of metal ions in solution rather than reduced sorbent efficiency. The near-constant total uptake across all doses indicates that adsorption occurs under ion-limited conditions, where sufficient active sites are available to capture nearly all ions present. Similar results were seen for MSP and DSP phosphate composites, which used a lower solid mass weight of 0.01 g of both adsorbents to reach maximum Yb^{3+} ion adsorption of 90 and 95 mg g^{-1}, respectively.

3.2.4. Influence of Yb^{3+} concentrations and adsorption temperature. The adsorption process and the movement of ions between various solution feeds and functional groups on the composite surfaces are significantly influenced by the concentration of metal ions. Thus, utilizing additional constant

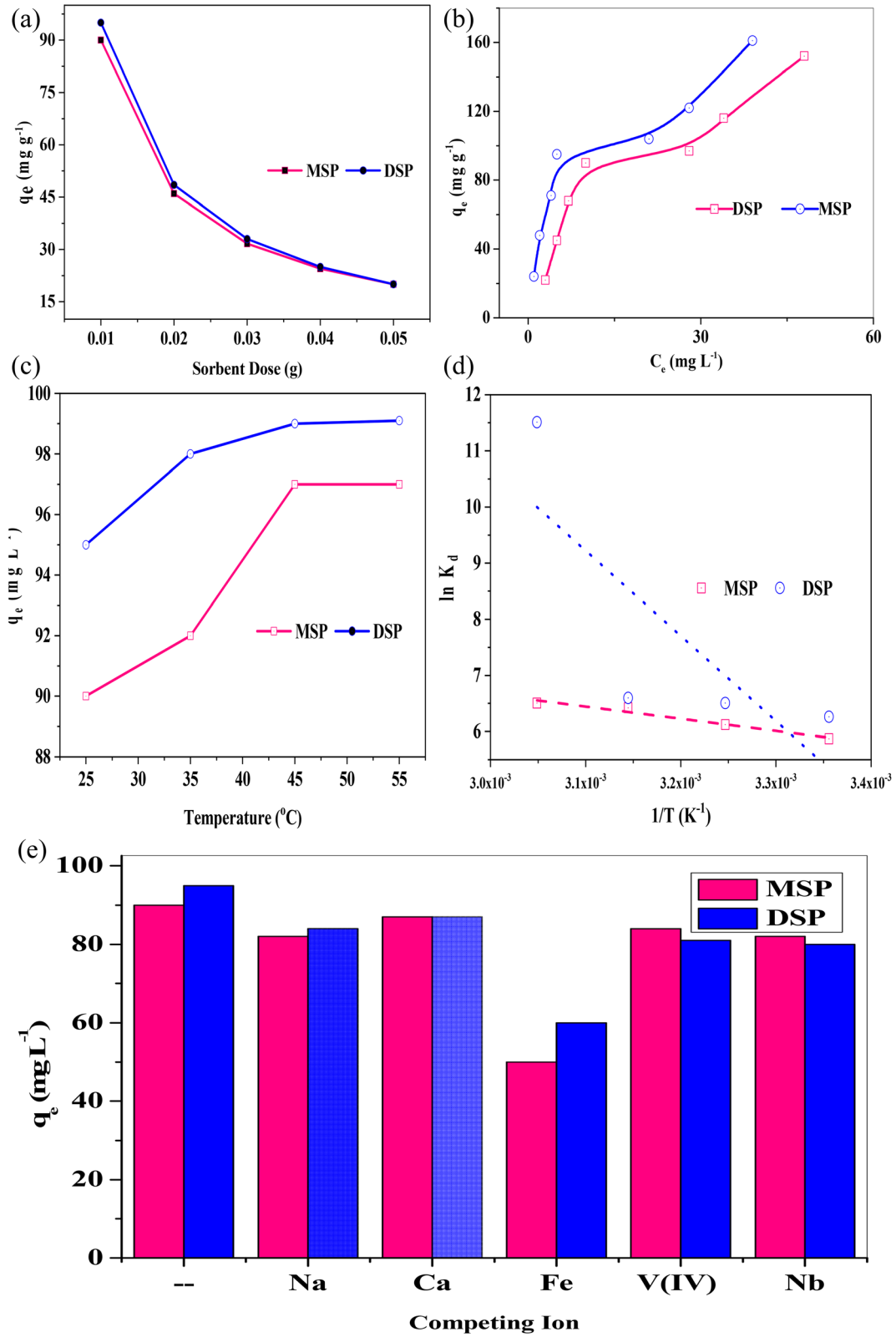

Fig. 8 (a) Sorbent dose impact, (b) metal ion concentration impact, (c) adsorption temperature impact, (d) 1/*T versus* ln K_d curve, and (e) competing ions impact.

conditions as indicated in Table 1, the impact of ytterbium ion concentrations ranging from 25 to 200 mg L^{-1} on the adsorption of MSP and DSP phosphate compounds was investigated, as illustrated in Fig. 8b. Increasing the concentration of metal ions demonstrated the strong adsorption performance of Yb^{3+} on phosphate resins. This may be expected given the rise in

Table 3 Thermodynamic parameters for Yb^{3+} sorption onto the MSP and DSP composites

			$\Delta G°$ kJ mol^{-1}			
			Temperature, K			
Sorbent	$\Delta H°$ kJ mol^{-1}	$\Delta S°$ J mol^{-1} K^{-1}	298	308	318	328
MSP	17.960	109.16	−14.569	−15.661	−16.752	−17.844
DSP	12.603	467.166	−126.612	−131.284	−135.956	−140.627

concentration and, as a result, the pushing force movement towards the active areas.[53] The negatively charged particles on the composite active sites were strongly attracted to the high concentration of Yb^{3+} ions. To put it another way, the increased potentiality of binding with the authorized active sites concentrated on the composite was responsible for the improvements in the adsorption of metal ions by raising their initial concentrations. Using a metal ion concentration of 200 mg L^{-1}, sharp adsorption of Yb^{3+} ions of 152 and 161 mg g^{-1} was accomplished on MSP and DSP resins, respectively.

It was evident from Fig. 8c that the adsorption of Yb^{3+} ions on phosphate resins was enhanced by reaction temperatures between 298 and 323 K with constant factors of 10 mg of solid sorbent, 10 mL of feed solution with metal ion concentrations of 100 mg L^{-1}, adsorption time of 45 min, and pH of 4.0. The positive factor gained from raising the adsorption temperatures led to an increase in the kinetics of the reactants from external interventions to reach the activation energy required for the molecule to undergo and enhance the adsorption process. From the temperature effect curves shown in Fig. 8c, mild enhancement in the adsorption of Yb^{3+} ions on MSP and DSP resins was found to range from 90 and 95 mg g^{-1} to 97 and 99.1 mg g^{-1} by varying the adsorption temperature from 298 to 323 K respectively. These enhancements in adsorption by increasing temperatures were preliminary evidence of the chemical nature of the adsorption processes of Yb^{3+} ions on MSP and DSP phosphate resins.[54]

3.2.5 Adsorption thermodynamic. Eqn (8) was used to display $\ln K$ *vs.* $1/T$ for the adsorption processes of Yb^{3+} onto phosphate sorbents, as illustrated in Fig. 8d. This resulted in straight lines with intercept and slope equal to $\Delta S°/R$ and $\Delta H°/R$. Table 3 displays the computed thermodynamic coefficients $\Delta S°$, $\Delta G°$, and $\Delta H°$. The endothermic character of the adsorption reactions of ytterbium onto the functional groups scattered on the surface of both compounds was demonstrated by the positive values of $\Delta H°$ for adsorption, which favored an external energy source and showed a positive effect with increasing temperature. Furthermore, the unpredictability of the system that emerged in the adsorption processes between Yb^{3+} ions and the active sites on the surfaces of MSP and DSP is shown by the positive $\Delta S°$ values. On the other hand, using eqn (9), negative $\Delta G°$ values show that a high degree of interaction between metal ions and functional groups scattered on the sorbent surfaces is feasible, spontaneous, and directly beneficial. Ultimately, it was evident that entropic changes dominated the adsorption by calculating the values of $T\Delta S°$, which clearly reduced from the values of $\Delta H°$ with the change in the temperatures of the adsorption processes.[34,55] Although adsorption is often exothermic, the positive $\Delta H°$ values obtained in this study indicate an endothermic process, which is attributed to the energy required for partial dehydration of hydrated metal ions prior to their coordination with functional groups of the polymeric network. The positive $\Delta S°$ values suggest increased disorder at the solid-solution interface, likely due to the release of bound water molecules during adsorption. Consequently, the adsorption process is spontaneous and entropy-driven, as confirmed by the negative $\Delta G°$ values.[56]

3.2.6 Effect of competing ions. The ability of the synthesized sorbent to selectively extract the Yb^{3+} ions in the presence of the other ions was determined by examining the competing effect of other elements on the adsorption efficiency of Yb^{3+} ions. The fixed outcome circumstances described throughout this study 0.01 g of sorbent, swirling for 45 minutes at room temperature in 10 mL of acidic solution with pH 4.0 containing 100 mg L^{-1} of Yb^{3+} ions were used to conduct competing effect investigations. A specific concentration of several metal ions (Na^{+}, Ca^{2+}, Fe^{3+}, V^{4+}, and Nb^{5+}) combined with Yb^{3+} ions of the same concentration in an aqueous chloride solution. The adsorption of Yb^{3+} ions on the DSP composite was significantly impacted by other metal ions, particularly iron, which significantly decreased the adsorption efficiency to half, according to the competing experiments and the adsorption data displayed in Fig. 8e. On the other hand, the presence of Na^{+}, Ca^{2+}, V^{4+}, and Nb^{5+} ions was found to have a minor impact on the adsorption of ytterbium ions on MSP. Furthermore, it was found that only iron significantly affected the adsorption of both MSP and DSP for Yb^{3+} ions. This could be explained by the fact that both iron and ytterbium are trivalent ions (as seen in the MEDUSA curve Fig. 7b) and that their strong similarity during interaction with solid adsorbents may account for their fierce competition for the active sites on the surface of the composites. Selectivity toward Yb^{3+} was quantified by evaluating the relative adsorption capacity and selectivity coefficients in the presence of competing ions. Both MSP and DSP composites retained more than 80% of their Yb^{3+} uptake in multi-ion systems, confirming strong preferential adsorption driven by specific coordination with phosphate functionalities.

3.3. Adsorption mechanism

Prior to radiation, a number of esterification reactions between acrylic acid and mono- and di-sodium phosphate are anticipated. As seen in Fig. 9, the mixture contained numerous substances

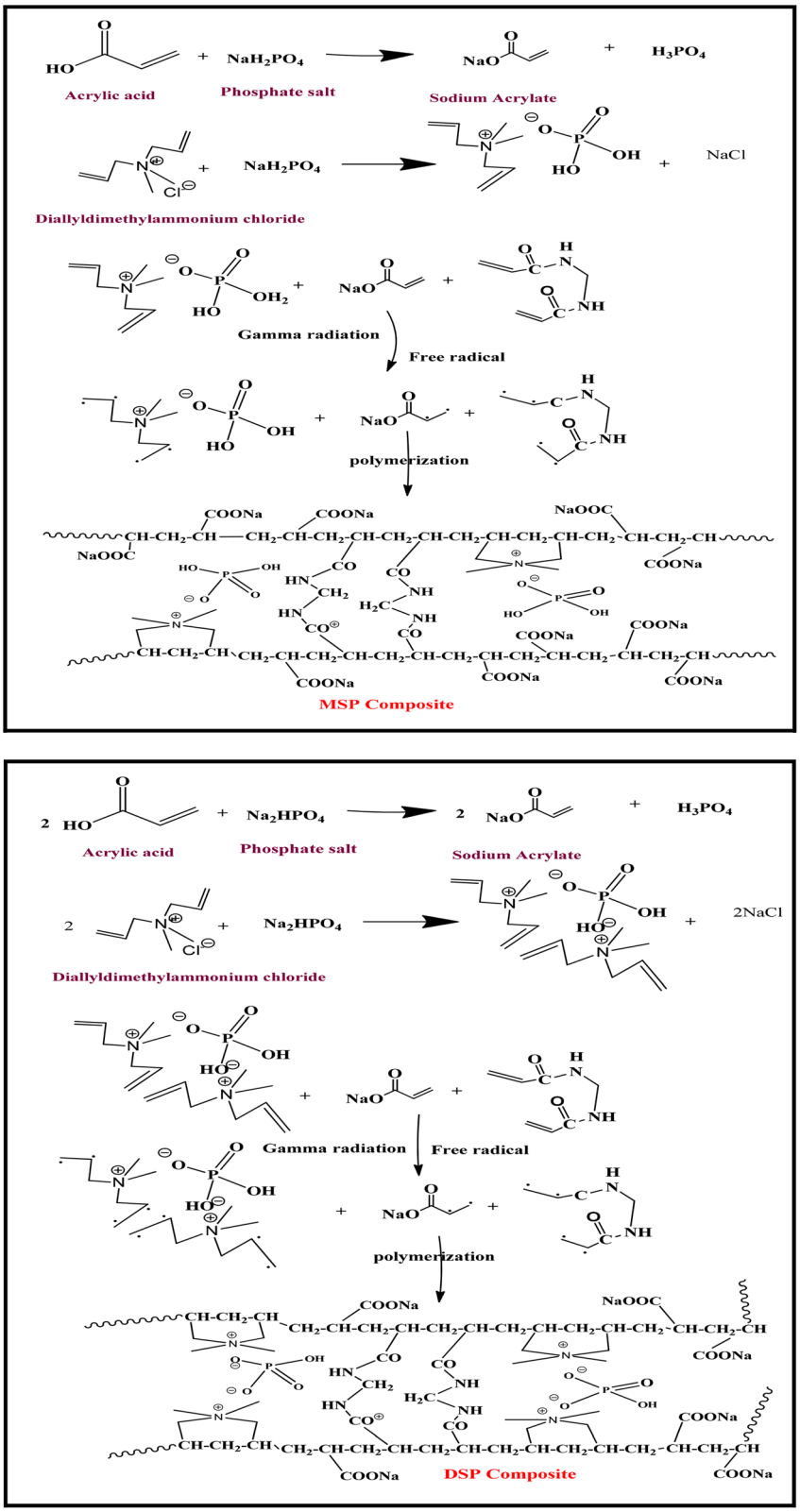

Fig. 9 A suggested diagram for the preparation and the polymerization of the MSP and DSP composites.

before to gamma irradiation, including phosphoric acid acrylate, allyl alcohol, and MBA linker. Many double bonds in phosphoric acid acrylate, allyl alcohol, and MBA linker were broken as a result of radiation exposure, producing a comparatively significant number of free radicals that led to polymerization and the creation of the suggested phosphate absorbers. With

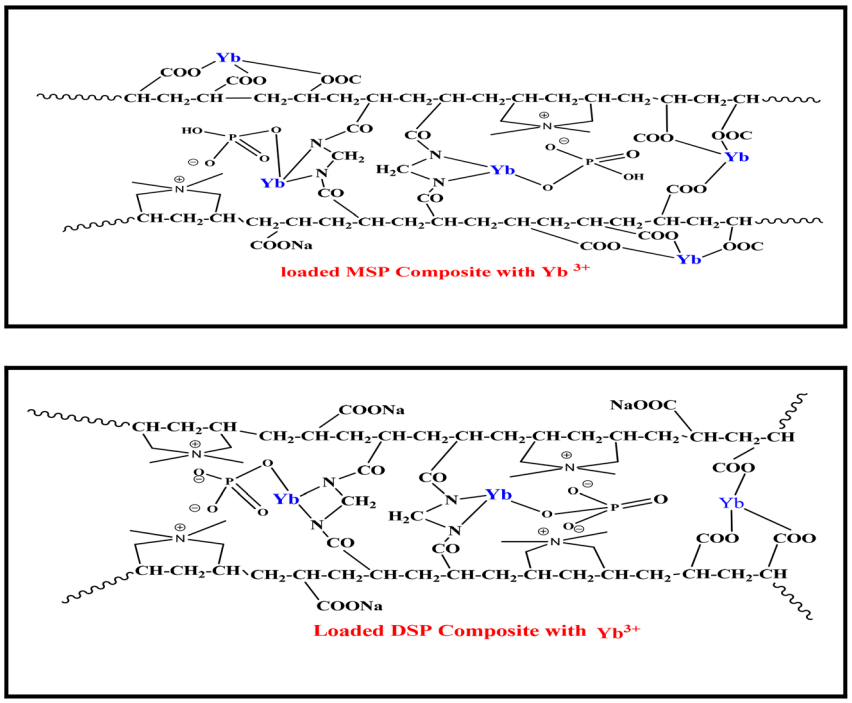

Fig. 10 The prediction mechanism for the adsorption of Yb^{3+} ions upon the MSP and DSP composites.

minimal interference from MBA in the crosslinking and tangling between the synthetic resin layers, the phosphate composite structure was anticipated to be constructed by polymerization using acrylic compounds and allyl alcohol as monomers. Numerous functional groups, including carboxylic (–COOH), hydroxyl (–OH), and phosphate groups (–$PO(OH)_2$ or –PO(OH)–), were present in both synthesized sorbents, suggesting the presence of dense active sites on the surface of the produced MSP and DSP that could draw in ytterbium ions. As seen in Fig. 10, an electrostatic attraction between these groups and Yb^{3+} ions has previously been proposed. The coordination chemistry of rare earth element extraction with acidic organophosphorus extractants such as D2EHPA and TBP is well-established in liquid–liquid extraction systems, where REE ions form inner-sphere complexes with oxygen donor ligands and undergo ion-exchange mechanisms involving proton displacement. Recent studies have shown that D2EHPA extracts rare earth ions through coordination of the phosphoryl oxygen to the metal center, with the process describable by equilibrium complexation and ion-exchange reactions with REE species in solution. Functional materials inspired by these extractants, such as phosphate-functionalized mesoporous supports, similarly leverage oxygen-donor ligands to coordinate REE^{3+} ions, reflecting the underlying HSAB (hard acid–hard base) interactions observed in LLE. This parallel supports the mechanistic interpretation of phosphate groups in sorbents acting as hard Lewis bases that preferentially bind REE^{3+} ions *via* surface coordination bonds.[57,58]

3.4 Desorption, recycling and stability studies results

Sulfuric acid and hydrochloric acid, two mineral acids with varying concentrations of 0.5 and 1 mol L^{-1}, were examined in order to extract Yb^{3+} ions from the loaded MSP and DSP composites. First, both concentrations of hydrochloric acid and sulfuric acid were used to compare their efficacy. Second, the recovery of ytterbium ions from the loaded composites was more effective at larger concentrations of both acids. Consequently, 1.0 mol per L HCl was the ideal leaching solution, as shown in Fig. 11a, yielding adsorption efficiencies of 95 and 93.9% for Yb-loaded MSP and DSP resins, respectively. The desorption processes were carried out at room temperature using 0.05 g of Yb-loaded resin, 10 mL of elute solution, and a 30-minute stirring duration at 300 rpm. Several soaking tests in acidic and alkaline solutions were used to investigate the stability of the phosphate composites. The remaining compounds were filtered, dried at 333 K for 6 hours, weighed, and then compared to their initial weights. Concentrations of 0.25 and 0.5 mol L^{-1} of HCl and NaOH were investigated separately as soaking solutions for the composite resins with other constant conditions, such as soaking time for 24 hours. The remaining mass percentages of various phosphate sorbents after soaking in various solutions are displayed in Fig. 11b, which highlights the impact of breakdown using sodium hydroxide as the soaking solution, particularly at the concentration of 0.5 mol L^{-1}. Their forms, hues, and molecular swelling all changed in tandem with these decomposition events. Both the two compounds' primary structures and the distribution of their functional groups may be significantly impacted by this. As a result, it was determined not to use sodium hydroxide to exchange the two chemicals. Hydrochloric acid, on the other hand, barely affects phosphate composites and does not alter their morphology. Rare mass losses of MSP and DSP resins employing 0.25 and 0.5 mole per L were seen in

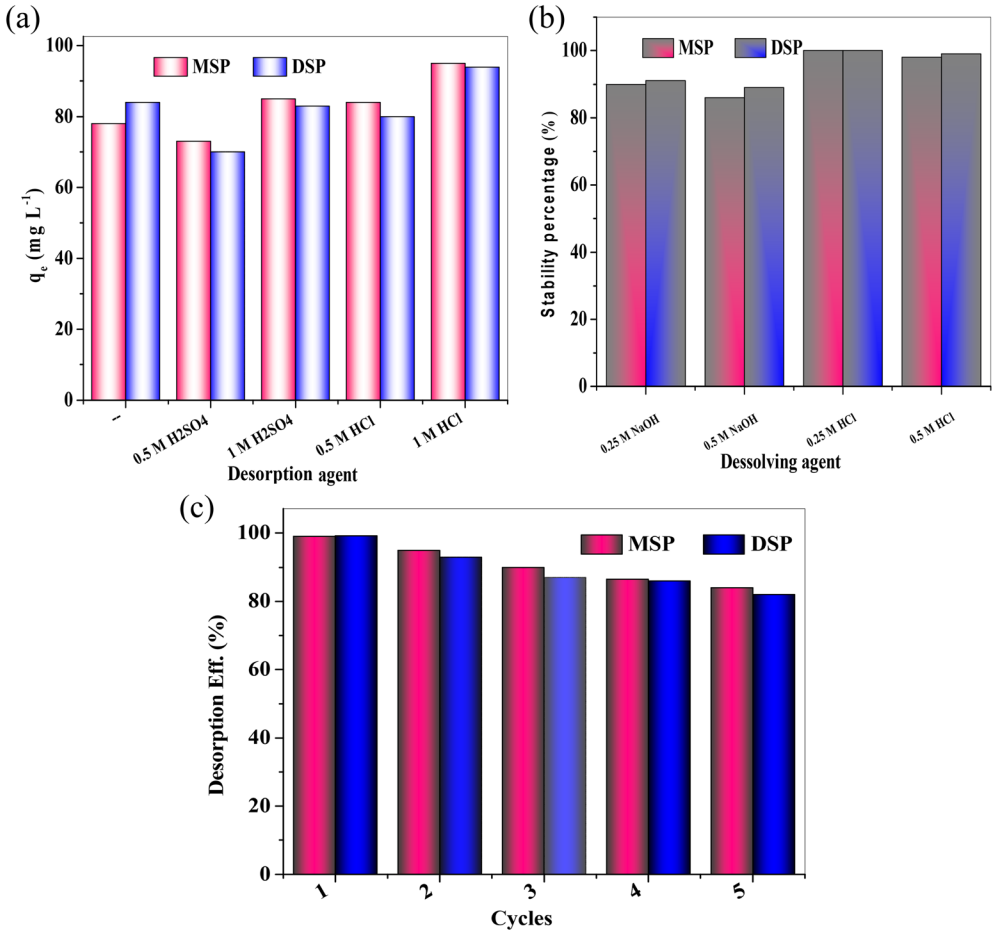

Fig. 11 (a) Desorption efficiencies of Yb^{3+} ions and (b) soaking results, and (c) recycling results of MSP and DSP composites.

Table 4 Ytterbium ions concentrations in the mineralizing fluids before and after the adsorption on the MSP and DSP composites

			MSP composite			DSP composite		
Sample	Initial conc.	Yb conc. before ads.	Yb conc. after ads.	Yb adsorbed, mg g^{-1}	Recovery eff., %	Yb conc. after ads.	Yb adsorbed, mg g^{-1}	Recovery eff., %
First concentrates	460	230	180	**50**	21.7	170	**60**	26.1
Second concentrates	920	300	250	**50**	16.7	230	**70**	23.3

Fig. 11b, suggesting that the chloride medium was the best option for using adsorption and desorption procedures.

Reusing MSP and DSP resins in various sequential ytterbium ion adsorption and desorption methods has been investigated. A slight and sequential decline in the recovery efficiencies of ytterbium ions for both composites was found when the adsorption and desorption processes were carried out under the optimal operating conditions determined during the investigation, as indicated by Fig. 11c, which shows the recovery percentage in each stage. Following the fifth recovery stage, the recovery efficiency values for MSP and DSP composites were 84 and 82%, respectively. The gradual decrease (~20%) in adsorption capacity after five cycles is attributed to partial irreversible binding of metal ions to high-affinity phosphate sites and minor pore blockage, while the preservation of ~80% capacity confirms the structural stability and reusability of the porous polymer networks. This moderate loss in capacity is consistent with literature reports for phosphate-based polymer adsorbents, where partial pore fouling or incomplete desorption can occur.[56,59] Overall, these results demonstrate that both MSP and DSP composites exhibit good structural stability and recyclability, making them suitable for repeated use in practical adsorption applications.

Table 5 Comparative study of different adsorbent materials for Yb^{3+} ions

Adsorbent	Max. adsorption capacity (mg g^{-1})	pH	Temp (°C)	Ref.
Ivy leaves marc (ILM)	169	5.0	25	63
Tulsion CH-96 resin	Comparable to DEHPA and EHEHPA	4.5	30	64
Ionic liquid-impregnated resin	—	6.0	25	65
Gel-type weak acid resin (110 resin)	265.8	5.5	25	66
3-Amino-5-hydroxypyrazole impregnated bleaching clay (AHIBC)	171.32	6.0	25	67

3.5. Real application results

Investigations were conducted into the potential of MSP and DSP phosphate composites as adsorbents for ytterbium ions from chloride feed solutions obtained from NMA laboratories that contained numerous competing ions. Feed solutions made from concentrates that needed to be removed utilizing the best regulatory requirements affecting adsorption showed respectable ytterbium ion concentrations. After digesting the two mineralization samples with hydrochloric acid, the feed solutions were made at concentrations of 460 and 920 mg L^{-1}. They were then diluted to 230 and 300 mg L^{-1}, respectively, to adjust their pH to the ideal adsorption conditions. The best adsorption conditions were used, including feed pH 4.0, 0.01 g of phosphate sorbent, 10 mL of acidic solution, and 45 minutes of room temperature stirring. The concentrations of ytterbium ions in the mineralizing fluids before to and following the adsorption on the MSP and DSP composites were shown in Table 4. Undoubtedly, the adsorption of ytterbium was significantly reduced on MSP and DSP compounds from 90 and 95 mg g^{-1} to 50 and 60 mg g^{-1} for the first feed solution and 50 and 70 mg g^{-1} for the second solution, respectively. These reductions could be attributed to the enormous concentrations of interfering ions present in the mineralizing fluids as cations and with concentrations several times greater than the desired element. Therefore, the high presence of competing positive ions and the limited active sites on the surface of the absorbent material led to a fierce competition between their huge concentrations and the low content of the desired element. Moreover, the low adsorption efficiency of phosphate composites requires further recovery processes through sequential contacts between acidic liquids and the studied compounds. Lastly, it was shown that both synthetic molecules could distinguish ytterbium ions from other competing ions. The eluent solutions of low competing ion contents can be subjected to further refining stages using the oxalic acid precipitation technique,[60–62] which could achieve the ultra-purification processes for ytterbium contents. Comparing the different adsorbents in terms of their ability to recover ytterbium ions, as shown in Table 5, it was clear that both radioactive materials are effective in recovering ytterbium from fluid solutions.[63–67]

4 Conclusion

MSP and DSP phosphates were sufficiently polymerized and investigated as a novel adsorbents for Yb^{3+} ions. The produced adsorbents' chemical and physical characteristics were examined to verify their organophosphorus structure, show that polymerization was successful, identify the presence of multifunctional groups on their structures, and verify that adsorption had taken place. Additionally, 90 and 95 mg g^{-1} of ytterbium were adsorbed on the mono- and di-phosphate composites, respectively, under the ideal adsorption conditions, which included 0.01 g of sorbent, stirring for 45 minutes at room temperature, and 10 mL of an acidic solution of pH 4.0 containing 100 mg L^{-1} of Yb^{3+} ions. The chemical character of metal ion adsorption processes and their direct relation with temperature have been shown by kinetic modeling investigations of ytterbium ion adsorption processes on phosphate resins. Furthermore, the results of thermodynamics demonstrated the endothermic characteristics of the adsorption processes. Ultimately, the efficacy of recovering the element's ions in the presence of numerous other elements was demonstrated, indicating the possibility of using the two composites made by free radical polymerization containing functional phosphate groups as absorbent materials for ytterbium ions. This confirmed the possibility of extracting the ytterbium content from chloride solutions of the concentrates of the two regions.

Ethical statement

The authors confirm that the manuscript has been read and approved by all authors. The authors declare that this manuscript has not been published and not under consideration for publication elsewhere.

Consent to participate

All of the authors consented to participate in the drafting of this manuscript.

Consent for publication

All of the authors consent to publish this manuscript.

Author contributions

All authors contributed to the study conception and design, material preparation, data collection and analysis. All authors read and approved the final manuscript.

Conflicts of interest

The authors declare that they have no conflict of interest.

Data availability

All the data used for this work are available upon request.

References

1 W. M. Haynes, *CRC Handbook of Chemistry and Physics*, CRC Press, Boca Raton (FL), 95th edn, 2015.
2 J. S. Coursey, D. J. Schwab, J. J. Tsai and R. A. Dragoset, *Atomic Weights and Isotopic Compositions (Version 4.1)*, National Institute of Standards and Technology, Gaithersburg (MD), 2015.
3 J. Emsley, *Nature's Building Blocks: an A–Z Guide to the Elements*, Oxford University Press, New York, 2nd edn, 2011.
4 U.S. Geological Survey, *Mineral Commodity Summaries*, US Geological Survey, Reston (VA), 2021.
5 R. Halmshaw, *Industrial Radiology: Theory and Practice*, Springer, Berlin, 1995, pp. 168–169.
6 J. Emsley, *Nature's Building Blocks: an A–Z Guide to the Elements*, Oxford University Press, Oxford, 2003, pp. 492–494.
7 G. Zhao, L. Su, J. Xu and H. Zeng, Response to comment on efficient diode-pumped Yb:Gd_2SiO_5 laser, *Appl. Phys. Lett.*, 2007, **90**(6), 066103, DOI: 10.1063/1.2435314.
8 D. Hayes, Entanglement of atomic qubits using an optical frequency comb, *Phys. Rev. Lett.*, 2010, **104**(14), 140501, DOI: 10.1103/PhysRevLett.104.140501.
9 E. C. Koch and A. Hahma, Metal-fluorocarbon pyrolants XIV: High density-high performance decoy flare compositions based on Yb/PTFE/Viton®, *Z. Anorg. Allg. Chem.*, 2012, **638**(5), 721.
10 A. Weberg, M. Dembowski, Q. K. Blad, G. S. Goff, S. K. Hanson and I. May, Scaling high-speed counter-current chromatography for preparative neodymium purification: insights and challenges, *J. Chromatogr. A*, 2024, **1729**, 465033, DOI: 10.1016/j.chroma.2024.465033.
11 S. V. S. H. Pathapati, M. L. Free and P. K. Sarswat, A comparative study on recent developments for individual rare earth elements separation, *Processes*, 2023, **11**, 2070, DOI: 10.3390/pr11072070.
12 O. A. Desouky, A. M. Daher, Y. K. Abdel-Monem and A. A. Galhoum, Liquid-liquid extraction of yttrium using Primene-JMT from acidic sulfate solutions, *Hydrometallurgy*, 2009, **96**, 313.
13 D. K. Singh, H. Singh and J. M. Mathur, Extraction of rare earths and yttrium with high molecular weight carboxylic acids, *Hydrometallurgy*, 2006, **81**, 174.
14 J. N. Mathur and G. R. Choppin, Paraffin wax as a diluent for extraction of actinides and lanthanides with TBP, *Solvent Extr. Ion Exch.*, 1998, **16**, 459.
15 J. Z. Zhou, W. H. Duan, X. Z. Zhou and C. Q. Zhang, Application of annular centrifugal contactors in the extraction flowsheet for producing high purity yttrium, *Hydrometallurgy*, 2007, **85**, 154.
16 W. W. Wang, X. L. Wang, S. L. Meng, H. F. Li and D. Q. Li, Extraction and stripping of ytterbium(III) from H_2SO_4 medium by Cyanex 923, *J. Rare Earths*, 2006, **24**, 685.
17 S. Guoxin, C. Yu, J. Runtian, X. Rongqi and S. Sixiu, Extraction of Tb(III) with N,N,N′,N′-tetrabutylmalonamide, *J. Serb. Chem. Soc.*, 2002, **67**(10), 653–659.
18 Y. A. El-Nadi, N. E. El-Hefny and H. F. Aly, Solvent extraction and recovery of Y(III) and Yb(III) from fluorspar mineral, *Int. J. Miner., Metall. Mater.*, 2013, **20**(8), 713.
19 X. W. Huang, J. N. Li, Z. Q. Long, X. X. Xue, Y. Q. Zhang and Z. W. Zhu, Synergistic extraction of rare earth by mixtures of EHEHPA and D2EHPA from sulfuric acid medium, *J. Rare Earths*, 2008, **26**(3), 410.
20 Y. Q. Zhang, J. N. Li, X. W. Huang, C. M. Wang, Z. W. Zhu and G. C. Zhang, Synergistic extraction of rare earths by mixture of HDEHP and HEH/EHP in sulfuric acid medium, *J. Rare Earths*, 2008, **26**(5), 688.
21 Y. A. El-Nadi, Lanthanum and neodymium from Egyptian monazite: synergistic extractive separation using organophosphorus reagents, *Hydrometallurgy*, 2012, **119–120**, 23.
22 H. Sereshti, M. Kermani, M. Karimi and S. Samadi, Optimized ultrasound-assisted emulsification microextraction followed by ICP-OES for simultaneous determination of ytterbium and holmium in natural water, *Clean: Soil, Air, Water*, 2014, **42**(8), 1089–1097.
23 L. B. Jose, G. C. Silva and A. C. Q. Ladeira, Pre-concentration and partial fractionation of rare earth elements by ion exchange, *Miner. Eng.*, 2024, **205**, 108477, DOI: 10.1016/j.mineng.2023.108477.
24 S. Pramanik, S. Kaur, I. Popovs, A. S. Ivanov and S. Jansone-Popova, Emerging rare earth element separation technologies, *Eur. J. Inorg. Chem.*, 2024, **27**, e202400064, DOI: 10.1002/ejic.202400064.
25 X. L. Wang, L. Ye, H. Jing, Z. Z. Yu, L. L. Bo and B. L. Dong, Efficiency and mechanism of adsorption of low concentration uranium in water by extracellular polymeric substances, *J. Environ. Radioact.*, 2019, **197**, 81.
26 A. A. Eliwa and A. E. Mubark, Effective sorption of U(VI) from chloride solutions using zirconium silico-tungstate matrix, *Int. J. Environ. Anal. Chem.*, 2021, **103**(16), 4079–4097.
27 M. M. Rajmane, B. M. Sargar and S. V. Mahamuni, Solvent extraction separation of zirconium(IV) from succinate media with N-n-octylaniline, *J. Serb. Chem. Soc.*, 2006, **71**, 223.
28 G. Sharma, A. Kumar, M. Naushad, B. Thakur, D. V. N. Vo, B. Gao, A. A. Al-Kahtani and F. J. Stadler, Adsorptional-photocatalytic removal of fast sulphon black dye by using chitin-*cl*-poly(itaconic acid-*co*-acrylamide)/zirconium tungstate nanocomposite hydrogel, *J. Hazard. Mater.*, 2021, **416**, 125714.
29 M. K. Jha, A. Kumari, R. Panda, J. R. Kumar and K. Yoo, Review on hydrometallurgical recovery of rare earth metals, *Hydrometallurgy*, 2016, **165**, 2–26.
30 J. Y. Lee, A. A. Omran and M. M. Fawzy, Fergusonite-(Y) beneficiation from mineralised granitic dykes at Wadi Ra's Abdah area, NE Desert, Egypt, *Int. J. Min. Miner. Eng.*, 2022, **13**(3), 256–275.
31 M. F. Raslan and M. M. Fawzy, Mineralogy and physical upgrading of fergusonite-Y and Hf-zircon in pegmatite of

Abu Dob granite, Egypt, *Bull. – Tabbin Inst. Metall. Stud.*, 2018, **107**(1), 52–65.

32 G. A. Dakroury, E. A. A. El-Shazly, A. A. Eliwa, A. E. Mubark and K. M. El-Azony, Utilization of titanium nanocomposites as prospective materials for recycling of vanadium from waste solutions, *J. Mol. Liq.*, 2022, **365**, 120170.

33 Z. Marczenko and M. Balcerzak, *Separation, Preconcentration and Spectrophotometry in Inorganic Analysis*, Elsevier, Amsterdam, 2000.

34 A. A. Eliwa, A. E. Mubark, G. A. Dakroury, E. A. A. El-Shazly and K. M. El-Azony, Polyacryl-dimethyl-heptadecanamine-Mullite as a promising sorbent for chromium and vanadium sorption from ilmenite, *J. Environ. Chem. Eng.*, 2022, **10**, 108886.

35 S. I. Moussa, Z. A. Mekawy, G. A. Dakroury, A. M. Mousa and K. F. Allan, Linear and Non Linear Recognition for the Sorption of ^{60}Co and $^{152+154}$Eu Radionuclides onto Bio CuO Nanocomposite, *J. Polym. Environ.*, 2023, **31**, 2148.

36 H. J. Kreuzer and I. Tamblyn, *Thermodynamics*, World Scientific, Singapore, 2010.

37 K. V. Kumar and K. Porkodi, Mass transfer, kinetics and equilibrium studies for the biosorption of methylene blue using *Paspalum notatum*, *J. Hazard. Mater.*, 2007, **146**, 214.

38 A. E. Mubark, N. I. Falila, B. T. Mohamed and H. M. Salem, Functionalization of cellulose pentamine as a promising nano-amorphous sorbent for Zr(IV) and Hf(IV) ions recovery, *Can. J. Chem. Eng.*, 2025, **103**(6), 2813–2825.

39 M. Buchholz, I. Spahn, B. Scholten and H. H. Coenen, Cross-section measurements for the formation of manganese-52 and its isolation with a non-hazardous eluent, *Radiochim. Acta*, 2013, **101**, 491.

40 M. T. Colomer, Straightforward synthesis of Ti-doped YSZ gels by chemical modification of the precursors alkoxides, *J. Sol–Gel Sci. Technol.*, 2013, **67**, 135.

41 K. Malaie, O. Shojaei, S. Iranpour and Z. Taherkhani, Crystal growth inhibition of gypsum by a phosphino-polycarboxylic acid copolymer, *Heliyon*, 2021, **7**(1), e06064.

42 J. A. Schott, C. L. Do-Thanh, W. Shan, N. G. Puskar, S. Dai and S. M. Mahurin, FTIR investigation of CO_2 sorption mechanisms in porous ionic liquids, *Green Chem. Eng.*, 2021, **2**(4), 392–401.

43 A. A. Eliwa, Efficacious recovery of zirconium and yttrium ions from effluents using a gamma irradiated reduced graphene oxide polymeric composite, *J. Inorg. Organomet. Polym. Mater.*, 2023, **34**, 1150–1171.

44 B. Smith, *Infrared Spectroscopy: Fundamentals and Applications*, Boca Raton, CRC Press, 2011.

45 L. C. Ferguson and R. J. H. Clark, *Infrared and Raman Spectroscopy: Principles and Spectral Interpretation*, Elsevier, Amsterdam, 2016.

46 N. Yasir, A. S. Khan, N. Akbar, M. F. Hassan, T. H. Ibrahim, M. Khamis, R. Siddiqui, N. A. Khan and P. Nancarrow, Amine-Based Deep Eutectic Solvents for Alizarin Extraction from Aqueous Media, *Processes*, 2022, **10**, 794.

47 S. L. Williams, D. N. Beatty and W. V. Srubar, A small-scale thermogravimetric method to measure the chemical reactivity of supplementary cementitious materials, *Cement*, 2023, **12**, 100071.

48 H. Alamgholiloo, N. N. Pesyan, R. Mohammadi, S. Rostamnia and M. Shokouhimehr, Synergistic advanced oxidation process for the fast degradation of ciprofloxacin antibiotics using a GO/CuMOF-magnetic ternary nanocomposite, *J. Environ. Chem. Eng.*, 2021, **9**, 105486.

49 G. F. Oliveira, R. C. Andrade, M. A. G. Trindade, H. M. C. Andrade and C. T. Carvalho, Thermogravimetric and spectroscopic study (TG–DTA/FT–IR) of activated carbon from the renewable biomass source babassu, *Quim. Nova*, 2017, **40**(3), 284–292.

50 A. Ahmed, A. Singh, S. J. Young, V. Gupta, M. Singh and S. Arya, Synthesis techniques and advances in sensing applications of reduced graphene oxide (rGO) Composites: A review, *Composites, Part A*, 2023, **165**, 107373.

51 M. Banach, Z. Kowalski, Z. Wzorek and K. Gorazda, A chemical method of the production of "heavy" sodium tripolyphosphate with the high content of Form I or Form II, *Pol. J. Chem. Technol.*, 2009, **11**(2), 13–20.

52 A. N. Spiess and N. Neumeyer, Research article An evaluation of R^2 as an inadequate measure for nonlinear models in pharmacological and biochemical research: a Monte Carlo approach, *BMC Pharmacol.*, 2010, **10**, 6.

53 D. J. Kim, S. H. Han, S. G. Kim and M. Yamamoto, Effective Ionic Radius of Y^{3+} Determined from Lattice Parameters of Fluorite-Type HfO_2 and ZrO_2 Solid Solutions, *J. Am. Ceram. Soc.*, 1994, **77**(2), 597–599.

54 A. A. Eliwa, A. M. Abdel-Razik, M. S. Hagag and A. E. Mubark, Synthesis and characterization of low-cost zirconium nanocomposites as adsorbents for arsenazo III pollutant, *Water, Air, Soil Pollut.*, 2024, **235**, 706.

55 A. A. Eliwa, Potentiality of using Synthesised Zinc Tungstate Nanoparticles for Thoron and Arsenazo III Removal from Waste Solutions, *Int. J. Environ. Anal. Chem.*, 2022, **104**(17), 5023–5044.

56 X. Li, Q. Zhou and H. Yang, Ultrafast and Stable Adsorption–Desorption Performance for Recovery of Valuable Rare-Earth Ions using High-Density Polyacrylic Acid Brush-Grafted Polypropylene Fibers Optimized by RSM Models, *Ind. Eng. Chem. Res.*, 2020, **59**(16), 7746–7754.

57 O. Cheremisina, M. Ponomareva, V. Sergeev, Y. Mashukova and D. Balandinsky, Extraction of rare earth metals by solid-phase extractants from phosphoric acid solution, *Metals*, 2021, **11**, 991.

58 W. Su, J. Chen and Y. Jing, Aqueous partition mechanism of organophosphorus extractants in rare earth extraction, *Ind. Eng. Chem. Res.*, 2016, **55**(30), 8424–8431.

59 P. Bora, C. Bhuyan, A. R. Borah and S. Hazarika, Carbon nanomaterials for designing next-generation membranes and their emerging applications, *Chem. Commun.*, 2023, **59**, 11320–11336.

60 A. A. Eliwa, A. E. Mubark, N. A. Abdelfattah and E. A. El-Gawad, Maximizing the exploitation of phosphogypsum wastes using soaking technique with citric acid, recovering rare-earth and residual phosphate contents, *J. Cent. South Univ.*, 2022, **29**(12), 3896–3911.

61 W. M. Abdellah, W. G. M. Abdel, A. M. Yousif and A. E. Mubark, Alternative Process for Recovering Zirconium and Rare Earth Elements from Pre-processed Gabal El-Faliq Concentrate Pegmatite, *Min., Metall., Explor.*, 2025, **42**(1), 409–420.

62 A. H. El-Afandy, A. M. Yousif and A. E. Mubark, Subsequent Separation of Niobium (Nb), Thorium (Th), Rare Earth Elements (REEs), Zirconium (Zr), and Uranium (U) from Abu Rusheid Cataclastic Concentrate, South Eastern Desert, Egypt, *Radiochemistry*, 2022, **64**(2), 257–267.

63 A. M. Emara, E. M. Elsharma and I. M. Abdelmonem, Adsorption of ytterbium(III) ions on ivy leaves marc: isotherm, kinetic and thermodynamic studies, *J. Radioanal. Nucl. Chem.*, 2025, **334**, 227–237.

64 B. Kronholm, C. G. Anderson and P. R. Taylor, A primer on hydrometallurgical rare earth separations, *JOM*, 2013, **65**, 1321–1326.

65 X. Sun, B. Peng, Y. Ji and D. Li, The solid–liquid extraction of yttrium from rare earths by solvent (ionic liquid) impregnated resin coupled with complexing method, *Sep. Purif. Technol.*, 2008, **63**(1), 61–68.

66 Z. Zhanwang and X. Chunhua, Adsorption behavior of ytterbium(III) on gel-type weak acid resin, *J. Rare Earths*, 2011, **29**(5), 407–412.

67 M. E. Mahmoud, H. H. Abdel-Aal and A. M. Ismail, Adsorption of yttrium ions on 3-amino-5-hydroxypyrazole impregnated bleaching clay, *Appl. Sci.*, 2024, **11**(21), 10320.